Performance of Sharply Bent Acoustic Resonators at High Sound Levels

Bailey I. Goldstein,* David N. Ramsey,† Haocheng Yu,‡ Spencer H. Bryngelson,§ and K. K. Ahuja¶
Georgia Institute of Technology, Atlanta, Georgia 30332

https://doi.org/10.2514/1.J066497

This study examines the effect of a single, sharp 90 deg bend placed along the length of a quarter-wave resonator (QWR) on its sound absorption. 3D-printed QWRs were tested in a two-microphone impedance tube both with low-level, broadband noise (less than 100 dB re 20 μPa) and high-amplitude, discrete tones ranging from incident sound pressure levels of 120 to 148 dB re 20 μPa. At low sound levels (and herein, broadband noise), the QWR resonance frequencies and absorption coefficients depended only subtly on the location of the bend, changing a maximum of approximately 4 and 2%, respectively, relative to the lowest value. For high-amplitude discrete tones, at 134 dB and higher, the QWRs exhibited meaningful nonlinearities that depended on the bend location. Direct numerical simulations of two-dimensional model problems are presented, linking experimentally observed trends to acoustically induced vortex formation in the QWR interior.

Nomenclature

c	=	speed of sound, m/s
d	=	quarter-wave resonator channel height, mm
f	=	frequency, Hz
L	=	resonator overall length, mm
L_1	=	length from quarter-wave resonator inlet to bend, mm
L_2	=	length from quarter-wave resonator bend to closed end, mm
n	=	positive integer
$\hat{R}$	=	reflection coefficient
u'	=	acoustic velocity fluctuation
x	=	distance along impedance tube, m
α	=	absorption coefficient
α_{broad}	=	absorption coefficient (broadband noise)
Δ	=	change in absorption coefficient
θ	=	normalized acoustic resistance

I. Introduction

RESONANT sound absorbers (called *resonators* here) are employed in many engineering applications. Within the aerospace industry, resonators can damp destructive thermoacoustic instabilities in combustors [1–4] or absorb noise before its emission from aircraft engines via acoustic liners [5–7]. A single-degree-of-freedom (SDOF) acoustic liner consists of a core of hexagonal cells sandwiched between a porous face sheet and an impermeable backing plate. All cells in a SDOF liner typically exhibit similar resonance frequencies at which they perform well as sound absorbers (e.g., the blade-passing frequency of a nearby rotor), readily dissipating incident acoustic energy at these frequencies into energy of other forms. The details of this dissipation depend on several factors but could include the conversion of acoustic energy into vortical energy (typically occurring at the liner's face sheet) or into thermal energy through thermoviscous dissipation mechanisms (typically occurring along the various surfaces inside each resonator including the face sheet and honeycomb-cell walls). A double-degree-of-freedom liner has a second layer of cells of a different depth, tuned to absorb sound at an additional frequency. Such liners are typically designed to absorb sound at specific frequencies. However, an acoustic liner that performs well at multiple frequencies is desirable (see the work of Jones et al. [7] for a discussion of this as it relates to aircraft engines). To achieve this multifrequency target, we adapt a traditional acoustic liner.

A variable-depth liner can serve as a broadband acoustic liner, where the constituent resonators have varied lengths and thus different resonance frequencies. Galles et al. [8] saw that combining several resonant sound absorbers to form a broadband, variable-depth liner is not an exclusively modern practice (see, e.g., the work by Wirt [9] who studied geometries like those shown in Fig. 1). There have since been related investigations. A comprehensive review of this topic is beyond the scope of this paper, and only a select few documents closely related to the present work are discussed. The reader is directed to the work by Kreitzman and Jones [10] for broader discussion. A linear resonator liner is relatively lengthy, and a considerable amount of solid material is wasted, especially for low-frequency sound. Variable-depth liners can be more compact if the individual resonators are bent [10–12].

Individual resonators can be used in various applications, including the suppression of combustion instabilities. However, bent resonators are widely reported for their efficacy of absorbing low-frequency sound while remaining compact relative to the wavelengths they absorb [13–15]. In addition to a bent geometry, such resonators have been described as *labyrinthine*, *serpentine*, or *space coiling*. Aside from noise-control applications, similar geometries have been used to create flat acoustic lenses [16] and other structures used to manipulate sound propagation [17–19]. A review of applications was provided by Cummer et al. [20]. The work on sound transmission in curved ducts by Cummings [21] is quite relevant, and it could be leveraged when designing such structures.

This work focuses on quarter-wave resonators (QWRs) that contain a single 90 deg bend placed at various locations along their

Presented as Paper 2025–3748 at the 2025 AIAA Aviation Forum, Las Vegas, NV, June 21–25, 2025; received 20 October 2025; accepted for publication 24 January 2026; published online 31 March 2026.

*Graduate Researcher, BSMS Honors Program, Daniel Guggenheim School of Aerospace Engineering; bgoldstein31@gatech.edu. Member AIAA (Corresponding Author).

†Postdoctoral Fellow, Daniel Guggenheim School of Aerospace Engineering; Now: Air Force Science and Technology Fellow, AFRL. Member AIAA.

‡Graduate Research Assistant, School of Computational Science and Engineering, Daniel Guggenheim School of Aerospace Engineering. Member AIAA.

§Assistant Professor, School of Computational Science & Engineering, Daniel Guggenheim School of Aerospace Engineering, George W. Woodruff School of Mechanical Engineering.

¶Regents Professor at Daniel Guggenheim School of Aerospace Engineering; also Regents Researcher and Chief of Aerospace and Acoustics Technologies at Georgia Tech Research Institute (GTRI). Fellow AIAA.

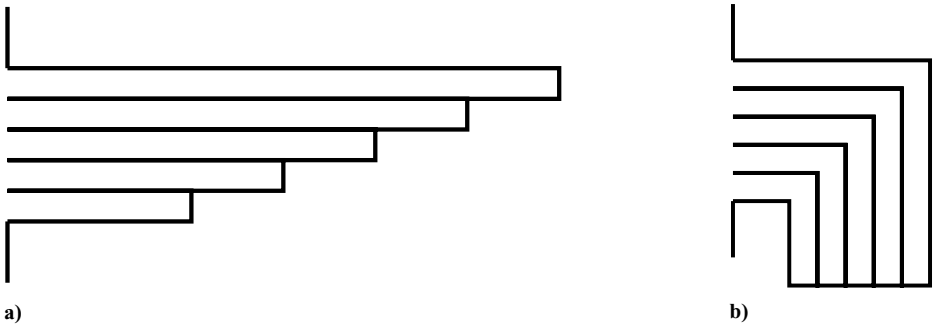

a) b)

Fig. 1 Illustrations of a) variable-depth liner and b) variable-depth liner with bent channels. Diagrams inspired by Wirt [9].

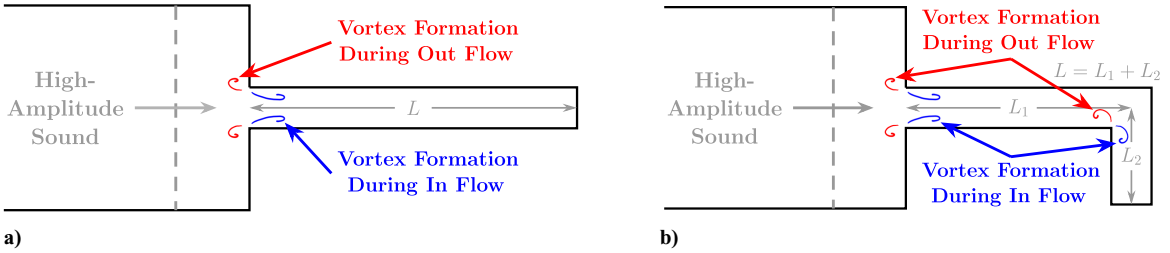

Fig. 2 Expected vortex formation for a QWR in the presence of high-amplitude sound: a) straight and b) bent.

length, with an emphasis on their behavior in the presence of high-amplitude sound. The QWR geometries of interest are sketched in Fig. 2. Figure 2a shows a straight QWR of length L. Sharp corners (like at the inlet of the QWR shown here) can give rise to large acoustically induced vortex formation when deployed in high-amplitude sound. The vortex formation during the phases of the acoustic oscillations, which result in an inflow and an outflow of gas to/from the QWR, is shown. This phenomenon changes the QWR performance [22,23]. Shown in Fig. 2b, additional vortex formation can occur inside a bent QWR, which is also of length L and with a bend at a distance L_1 from the QWR inlet as measured along its centerline. This effect could impact its acoustic performance, a finding supported by the results presented in this work.

The literature on these issues for bent resonators is scant. However, Sun et al. [24] found that QWRs containing multiple 180 deg bends exhibited meaningful vortex formation near the bends in the presence of high-amplitude sound. The present work investigates the effect of a single bend in detail for both low- and high-amplitude sound.

The remainder of this manuscript continues as follows. In Sec. II, prior literature on the behavior of resonators and other devices in the presence of high-amplitude sound is discussed. The bent QWR geometries studied in this paper, along with the experimental and computational methods, are described in Sec. III. Results are presented and discussed in Sec. IV, and concluding remarks are provided in Sec. V.

II. Background

Fundamentally, a resonator absorbs sound by dissipating incident acoustic energy into energy of other forms. For the configuration under study in this paper in the presence of sound at relatively low levels, this dissipation can typically be attributed mainly to viscous effects in the acoustic boundary layer along the resonator's interior walls [25]. However, other dissipative mechanisms exist and become especially important at sufficiently high sound levels. A dissipation mechanism known to occur in many geometries, largely visible in the presence of high-amplitude sound, is *acoustically induced vortex formation* [26–29]. With high sound levels, many have observed substantial acoustically induced vortex formation in and around resonators [4,30,31]. The added acoustic dissipation from these vortical structures depends on the sound amplitude, and the resonator's acoustic properties (i.e., impedance) [32] also depend on the sound amplitude. This phenomenon is colloquially referred to as a nonlinear effect. Similar phenomena are found for other geometries in the presence of high-amplitude sound, such as orifice plates [33–35].

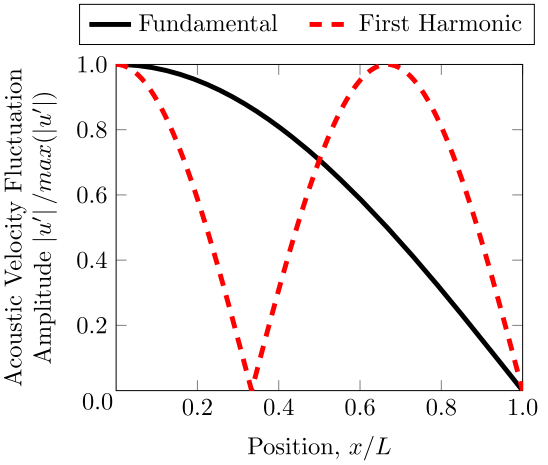

Fig. 3 Acoustic velocity fluctuation versus position along an ideal QWR at its fundamental and first harmonic resonance frequencies. The inlet is located at $x = 0$.

Figure 3 shows the acoustic velocity fluctuations inside an ideal QWR at its fundamental and first harmonic resonance frequencies with an open end at $x = 0$ (modeled as a pressure-release boundary) and a closed end at $x = L$, which is modeled as an acoustically rigid boundary. The amplitude of acoustic velocity fluctuations varies along the length of the QWR. At its fundamental resonance frequency, a velocity maximum exists at the resonator inlet. At its first harmonic, two maxima exist: one near the inlet and one around $x = 0.7L$. A QWR with a 90 deg bend is expected to exhibit similar acoustic velocity distributions and perform similarly to a straight QWR of equivalent length. However, QWRs with a bend near the velocity maxima are expected to show greater nonlinearity due to additional vortex formation on their interior (as introduced in Fig. 2b).

III. Methods

A. Test Articles

Figure 4 shows the nine different QWRs that were 3D-printed in clear resin using a Formlabs Form 3 stereolithography printer. Each QWR was tuned to have a nominal fundamental resonance

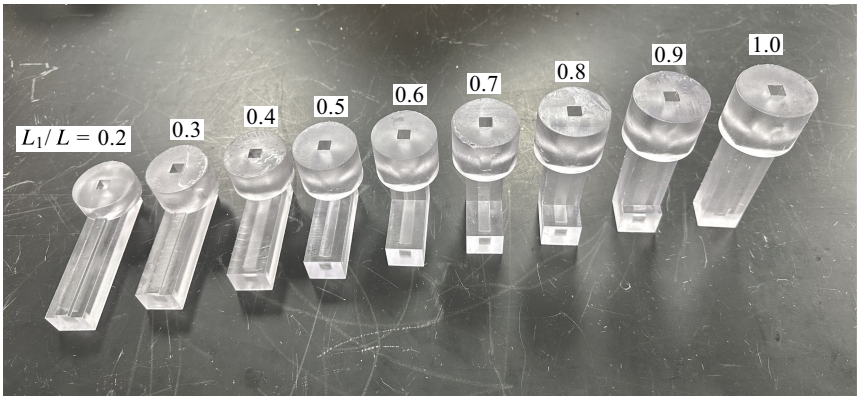

Fig. 4 3D-printed test articles. Solid cylinder not shown.

frequency of 1 kHz and thus an overall chamber length of 85.725 mm according to the formula for the nominal resonance frequencies of a QWR:

$$f(n) = \frac{(2n-1)c}{4L} \tag{1}$$

It is well established that the effective length of a QWR is slightly greater than its geometric length, and end corrections may be included to account for this. For simplicity, Eq. (1) contains no end correction. Each QWR had a square cross-section with a side length of 6.35 mm. To convey the placement of the 90 deg bend in a given test article, a length fraction L_1/L will be reported throughout. L_1 and L are also shown in Fig. 2 for reference. The printed QWRs range from a length fraction of 0.2 to 1.0 (straight QWR) in increments of 0.1, as shown in Fig. 4. One solid cylinder (not shown in Fig. 4) was printed and tested as a control to indicate the minimum sound absorption possible with the present setup.

B. Sound Absorption Measurements

A two-microphone impedance tube with an inner diameter of 28.58 mm was used for sound absorption measurements in broadband noise and discrete tones. A schematic of the setup is shown in Fig. 5. A JBL 2446J acoustic driver was located at one end, and the test article was installed at the other. An NI 4431 data acquisition device was used to output an excitation signal, which was then amplified and sent to the driver. Acoustic measurements were recorded using PCB 378A12 microphones at a sampling rate of 16384 Hz. Spectral analysis was conducted using Welch's method [36] applied to 16 384-point, Hanning-windowed blocks with 50% overlap between neighboring blocks, yielding a frequency resolution of $\Delta f = 1$ Hz.

When installing the test articles, a 3D-printed alignment guide plate was placed around the test article and bolted to the impedance tube to ensure the QWR was centered. Modeling clay was used to seal any potential small gaps between the impedance tube and the test article. Once the first test article was aligned and the modeling clay seal was established at the appropriate position, the alignment plate was no longer used for ease of testing. Because of their geometry, the bent QWRs studied here cannot be installed in a standard test-article holder. Nonetheless, the modeling clay seal was shown to be sufficient by measuring the sound absorption of a solid, 3D-printed cylinder test article as a control (not shown in Fig. 4). In theory, a perfectly rigid termination yields zero absorption; however, small nonzero absorption values are commonly observed in practice, consistent with the typical performance of this facility and attributable to unavoidable experimental imperfections, such as minor sealing losses and uncertainties in relative microphone phase calibration. A low measured absorption coefficient with this solid cylinder installed indicated a good-quality seal. Such measurements will be shown alongside the data for the QWRs.

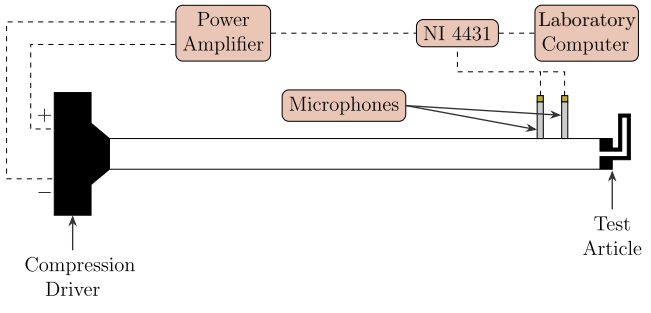

Fig. 5 Two-microphone impedance tube used in this study.

The data acquisition and processing routine followed American Society for Testing and Materials (ASTM) E1050 [37]. This setup included a microphone-swapping technique to determine a relative magnitude and phase calibration between the two microphones. Additionally, microphone sensitivities were measured using a 1 kHz tone. This absolute calibration was not required by the ASTM standard, but was needed to calculate the sound level in the tube. To ensure measurements with a high signal-to-noise ratio were recorded, the coherence between the two microphones was greater than or equal to 0.95 for all reported data points.

Measurements were made using both broadband noise and discrete tones. Each test article was exposed to low-amplitude, broadband noise, and 60 s microphone time histories were recorded during broadband measurements. For the discrete tones, a closed-loop controller automatically set the NI 4431 output voltage to achieve a tone of desired *incident* sound pressure level (ISPL) to within ±0.25 dB (a reference pressure of 20 μPa is used throughout), which was determined through a plane-wave decomposition technique [4,15]. The program automatically stepped through the desired frequency/ISPL ranges in prescribed step sizes, recording 7 s of microphone time history for each frequency/ISPL combination of interest. Each recording yielded the test article's absorption coefficient and impedance for that frequency/amplitude combination when processed according to ASTM E1050 [37].

C. Numerical Simulations

Direct numerical simulation (DNS) was conducted using the open-source code MFC [38–40], which includes the necessary acoustic source physics [41] and immersed boundary methods [42], among other useful physical features [43,44]. These simulations shed light on the vortex formation inside bent QWRs. Yu et al. [45,46] validated the use of MFC for studying the vortex formation phenomena in the presence of high-amplitude sound, where absorption coefficients of two-dimensional slit resonators in the work by Tam et al. [34] were reproduced by the numerical simulations. To reduce the computational cost of the DNS, we conducted two-dimensional (2D) simulations, as shown in Fig. 6, in which the immersed boundaries represent the full length of the QWR tested in

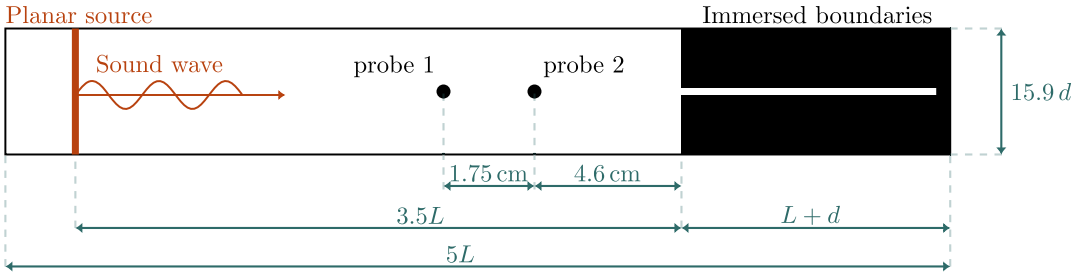

Fig. 6 Computational domain used for DNS. Only $L_1/L = 1.0$ is shown for brevity.

experiments. The two-dimensional problem cannot represent the three-dimensional (3D) physics, but it offers a simplified framework that captures the key mechanisms and qualitative trends observed in the experiments.

The QWR height is $d = 1.796$ mm, and the impedance tube height is $15.9d$. Although the DNS is 2D, this setup ensures that the impedance-tube-to-QWR area ratio matches the experimental setup. Maintaining this area ratio ensures that the two configurations exhibit similar reflection coefficients at the impedance-tube/QWR junction. (The unfamiliar reader can appreciate the importance of this area ratio upon applying the conservation equations in integral form across a sudden area change in a straight duct.)

Right-going acoustic waves were emitted from a planar acoustic source $3.5L$ from the incident face of the QWR ($0.5L$ away from the left domain boundary, which performs ghost cell extrapolation and is nonreflective). Dissipation of sound along the impedance tube walls was neglected, and these surfaces were set to be slip walls. The no-slip condition was enforced on the incident face of the QWR and all of its interior walls.

A uniform, structured mesh with equal cell side lengths was used with at least 10 cells across the acoustic boundary layer, as recommended by Tam et al. [47]. This mesh results in 40 cells across the opening of the QWR channel. A grid-refinement study revealed that doubling the number of cells has a negligible effect on the absorption coefficient, indicating that the grid resolution is sufficient for the present purposes. Numerical stability is ensured by maintaining the Courant–Friedrichs–Lewy number below 0.5. Table 1 summarizes the simulation configurations.

Two virtual probes separated by 1.75 cm sampled acoustic pressures at each time step. The closer probe (probe 2 in Fig. 6) is 4.6 cm away from the incident face of the QWR. The sampling frequency of the recorded time history equals the inverse of the simulation time step (0.1 μs increments). The duration of simulations is 0.1 s, equivalent to 100 cycles at the fundamental frequency. As has been done in prior works [47,48], the absorption coefficient was calculated using the procedure outlined in the ASTM standard [37].

D. Summary of Conditions Tested

For all nine QWR length fractions, sound absorption measurements were conducted in the presence of low-amplitude, broadband noise. Additionally, data were collected for the QWRs in the presence of high-amplitude tones. In the experiments, ISPLs from 120 to 148 dB were measured in steps of 7 dB. For each ISPL, a frequency sweep near the QWR resonance frequencies was conducted in 5 Hz steps. Correspondingly, 2D simulations were performed for three QWR length fractions (namely, $L_1/L = 0.4, 0.8$, and 1.0) with a 1 kHz tone at an ISPL of 120 and 148 dB. A DNS with broadband noise at an overall incident sound pressure level (OISPL) of 90 dB was used as a low-amplitude baseline. Table 2 summarizes the discrete tones for which experimental and computational results are presented in this paper.

Table 1 Simulation configuration of three different QWRs (the following simulations include cases with one broadband sound source at OISPL = 90 dB and two discrete tones at 1 kHz with ISPL = 120 dB and 148 dB, resulting in nine unique combinations)

QWR (L_1/L)	Domain size	Cell size (d/Δ_x)	Time step size (10^4 per cycle)	Time steps (cycles)
1	$238.92d \times 15.9d$	40	1	100
0.8	$230.68d \times 19.08d$	40	1	100
0.4	$211.58d \times 38.16d$	40	1	100

Table 2 Summary of test conditions using discrete tones (✓: experiments at fundamental and first harmonic; ✗: 2D computations at fundamental)

	QWR length fraction, L_1/L								
ISPL, dB	0.2	0.3	0.4	0.5	0.6	0.7	0.8	0.9	1.0
120	✓	✓	✓, ✗	✓	✓	✓	✓, ✗	✓	✓, ✗
127	✓	✓	✓	✓	✓	✓	✓	✓	✓
134	✓	✓	✓	✓	✓	✓	✓	✓	✓
141	✓	✓	✓	✓	✓	✓	✓	✓	✓
148	✓	✓	✓, ✗	✓	✓	✓	✓, ✗	✓	✓, ✗

IV. Results

The results are organized as follows. Sound absorption measurements obtained in the presence of low-amplitude, broadband noise are presented in Sec. IV.A, followed by measurements made in the presence of high-amplitude, discrete tones in Sec. IV.B. Last, DNS results are presented in Sec. IV.C.

A. Low-Amplitude, Broadband Noise

Typical absorption spectra measured in the presence of broadband noise are shown in Fig. 7 for QWR length fractions of 0.5 and 1.0, as well as the solid cylinder measured as a hard-termination baseline. Absorption spectra were obtained for all other test articles but are not included in Fig. 7 for clarity. First, the spectrum measured using the solid cylinder appears below 0.1 at all measured frequencies. This protocol provides confidence in the test article's installation and sealing with the impedance tube. For the two QWRs, the three peaks in the absorption spectra correspond to the three lowest resonance frequencies. For the fundamental resonance frequency near 1 kHz, the absorption curves for the two QWRs are nearly identical. The peaks become more dispersed at the harmonics. The peak absorption values for all test articles are within 1.8 and 2.1% for the fundamental and first harmonic, respectively.

To highlight trends as a function of L_1/L, Fig. 8 summarizes the measured resonance frequencies (see ∘ markers) and corresponding peak absorption coefficients (see × markers) for all QWRs tested. Figure 8a shows information about the QWR fundamental resonance frequency. An interesting dependence of the resonance frequency on the bend location is seen. Lower length fractions (bends closer to the QWR inlet) are associated with higher resonance frequencies. In other words, the resonance frequency is higher when the bend is placed in a region where greater acoustic velocity fluctuations are expected, as seen in the *Fundamental* curve in Fig. 3. The absorption coefficient exhibits an opposite trend, being lower in locations with higher expected velocity fluctuations.

Figure 8b shows a similar plot for the first harmonic. Although there is no clear dependence of the peak absorption coefficient on

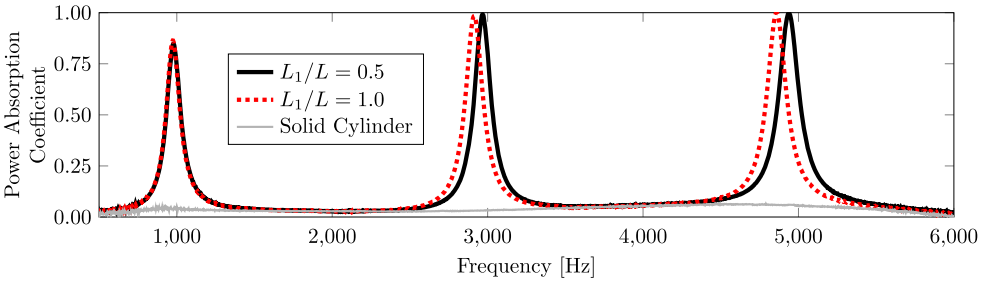

Fig. 7 Typical absorption spectra measured in the presence of low-amplitude, broadband noise.

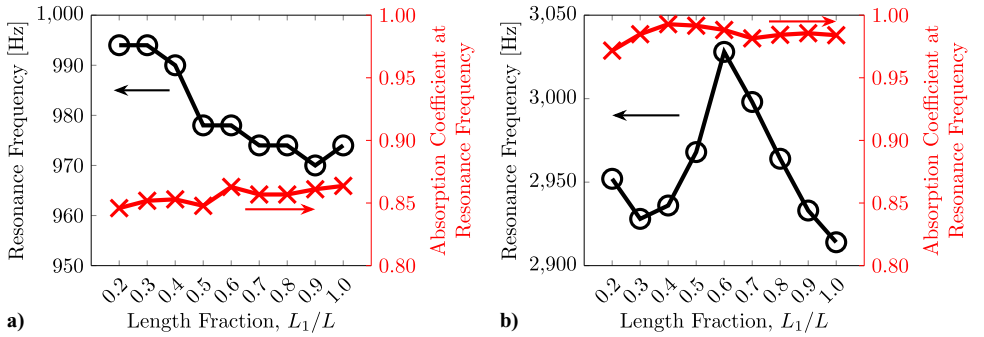

Fig. 8 A summary of the resonance frequencies and associated peak absorption coefficients for each L_1/L in the presence of broadband noise: a) fundamental and b) first harmonic.

the bend location, a clearer trend is visible in the resonance frequencies. The resonance frequency is highest when $L/L_1 = 0.6$ and is lowest for the straight resonator. This result, like the data corresponding to the fundamental resonance frequency, suggests that when a bend is placed in a region where acoustic velocity fluctuations are expected to be relatively high (see the *First Harmonic* curve in Fig. 3) the resonance frequency is higher than that for the straight QWR.

Others have also reported a small dependence of QWR resonance frequencies on the bend location. In a computational study, Catapane et al. [14] found that the resonance frequencies of QWRs containing N 180 deg bends deviated from expectations (the frequencies of Eq. (1)) only for high values of N. Cambonie et al. [49] observed that the elbow location in a pipe becomes important, as it is related to strong velocity gradients and can effectively shorten the total length of the pipe. Cambonie et al. [50] also found a small increase in resonance frequency in bent QWRs, though they were not sharply bent as in the present study. Overall, the broadband results shown in Fig. 8 suggest that the bend location can have an impact on the QWR performance, increasing the resonance frequency when the bend is located in a position where relatively high acoustic velocities are expected, though these effects are quite subtle.

The results in Fig. 8 indicate that, even at low amplitudes, the 90 deg bend's location has a subtle effect on the QWR resonance frequencies. As previously noted, the *effective* length of a QWR (the length which, when used in Eq. (1), produces resonance frequencies in agreement with experimental data) is different than its true physical dimension. For a typical, straight QWR, an *end* correction is added to its physical dimension. For all bent QWR geometries tested, the end correction would be the same. However, the results in Fig. 8 show that the resonance frequency is a function of L_1/L. This result suggests that an additional length correction (not having to do with end effects) may be needed for bent QWR geometries. Developing a method for calculating this correction is beyond the scope of this work and would be best examined using a larger number of test articles than those studied here.

B. High-Amplitude, Discrete Tones

Exemplar absorption coefficient measurements for a straight QWR ($L_1/L = 1.0$) exposed to high-amplitude tones are shown in Fig. 9. Figure 9a shows measurements near the QWR's fundamental resonance frequency. For an ISPL of 120 dB, the absorption coefficient was nearly identical to the low-amplitude, broadband

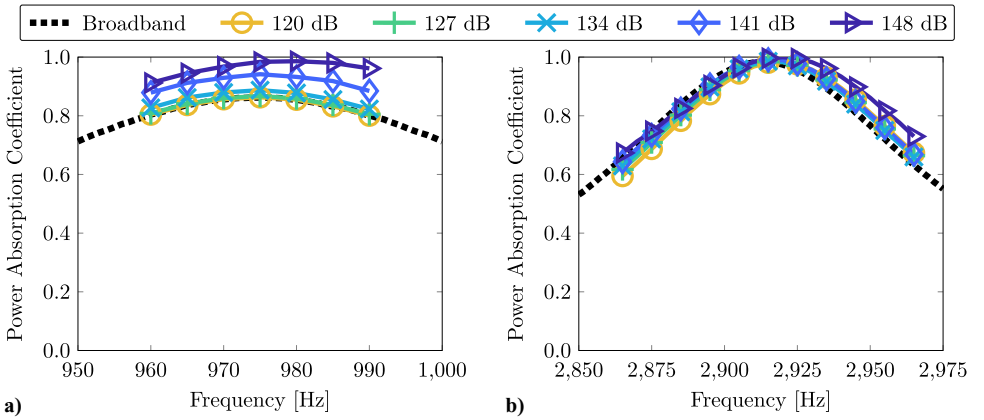

Fig. 9 Power absorption coefficient for the $L_1/L = 1.0$ (straight) QWR around the a) fundamental and b) first harmonic resonance frequencies as a function of ISPL.

measurements (see the dotted curve labeled *Broadband*). As the ISPL increases, so does the absorption coefficient. For the straight QWR, this result is attributed to an increasing effect of vortex formation at the inlet. Figure 9b shows similar measurements at the QWR's first harmonic. The absorption coefficient is less sensitive to ISPL than at the fundamental, being nearly unity even in the presence of low-amplitude, broadband noise.

The resonance frequencies of all QWRs in the presence of discrete tones are shown in Fig. 10. Figure 10a shows the fundamental resonance frequencies, and Fig. 10b shows the first harmonic. The results are similar to those identified with low-amplitude, broadband noise (see Broadband curves shown for reference). However, the resonance frequencies are only known to within ±2.5 Hz (the discrete-tone sweep was conducted in steps of five hertz). The placement of the bend again has little impact on the QWR's resonance frequencies. However, bends placed in regions of the QWR where relatively high acoustic velocity fluctuations are expected (see Fig. 3) lead to higher resonance frequencies.

Figure 11 shows the peak absorption coefficient values, which correspond to the resonance frequencies shown in Fig. 10. Absorption coefficients at the QWR's fundamental are shown in Fig. 11a, in which a large increase in the absorption coefficient with amplitude is seen for all length fractions. The absorption coefficients at the first harmonic are shown in Fig. 11b, in which the peak absorption coefficient is seen to increase with ISPL up to 141 dB and then decrease at 148 dB for $0.4 \leq L_1/L \leq 0.6$ while continuing to increase for other length fractions. These trends will be presented more clearly and discussed further in the next section.

To convey the trends in data from Fig. 11, a nonlinearity metric is defined as

$$\Delta \equiv \alpha - \alpha_{\text{broad}} \tag{2}$$

The resonance frequency varies with ISPL, as shown in Fig. 10. Thus, the values taken for α and α_{broad} (the broadband contribution) were the peak values associated with the resonance frequency of interest. Figure 12 shows the change in absorption coefficient Δ versus bend location at each measured ISPL. Figures 12a and 12b show these at the fundamental and first harmonic. These results show that Δ, a measure of the degree of nonlinearity exhibited by the QWR, depends on L_1/L. This result is elaborated on next.

If the bend placement did not affect the degree of nonlinearity exhibited by the QWR, then the Δ curves of Fig. 12 would show as horizontal lines for each ISPL, though this is not the case. Figure 12a shows that placing a bend closer to the QWR inlet, at the fundamental resonance frequency, leads to more meaningful nonlinear effects, measured here via Δ. The Δ curves for the first harmonic shown in Fig. 12b show a similar dependence of Δ on the bend placement, though the curves require additional interpretation provided in the following paragraph.

Figure 12b shows that, for an ISPL of 141 dB, the measured Δ is greatest for $L_1/L = 0.2$ and $L_1/L = 0.7$. These length fractions correspond to a bend where the acoustic velocities are expected to take their maximum values for the QWR's first harmonic. As shown in Fig. 11b, the absorption coefficient at the QWR's first harmonic approaches 1.0 for $0.4 < L_1/L < 0.6$ with an ISPL of 141 dB, and the absorption coefficients decreased for a yet higher ISPL of 148 dB. This result leads to a distinctive trend in the Δ plot shown in Fig. 12b. The largest decrease in Δ with an ISPL of 148 dB was found for the $L_1/L = 0.6$ QWR, which has a bend near the expected location of a velocity antinode inside the QWR. These changes highlight that a bent QWR can exhibit poorer performance as a sound absorber than a straight one, depending on the circumstance. More perspectives on this are discussed in Sec. V.

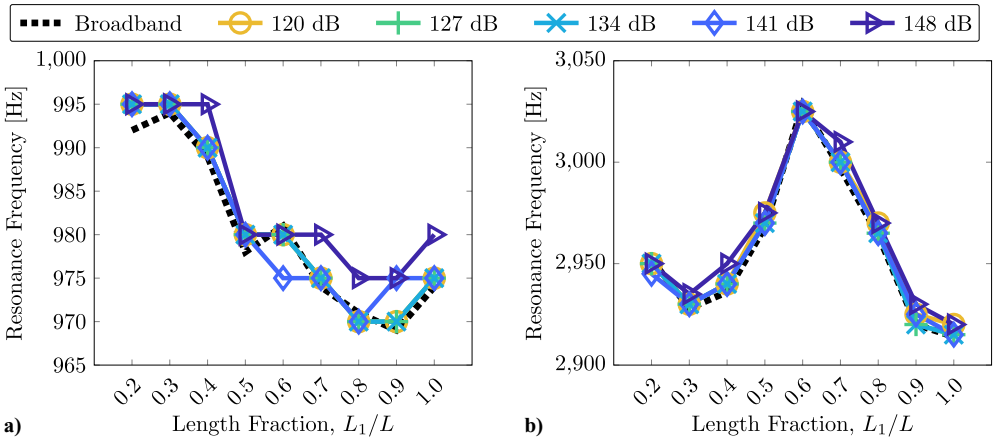

Fig. 10 QWR resonance frequencies as a function of discrete tone ISPL: a) fundamental and b) first harmonic.

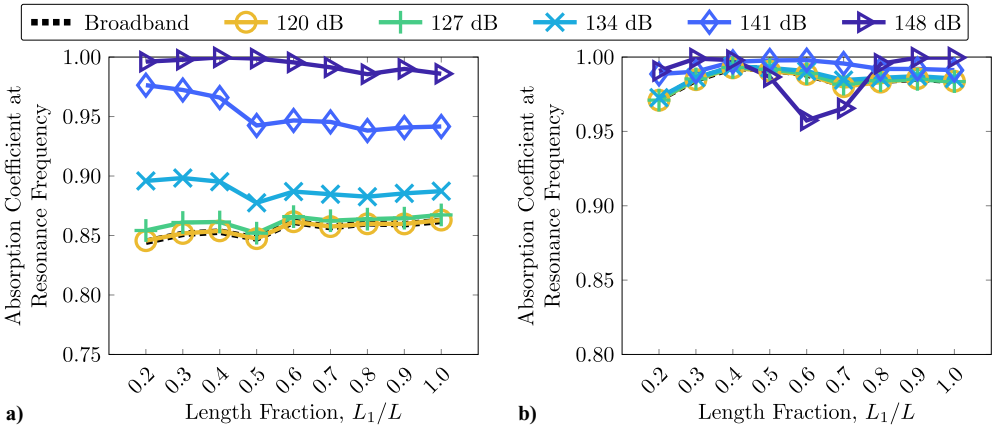

Fig. 11 QWR peak absorption coefficients in the presence of discrete tones at a) fundamental and b) first harmonic resonance frequencies.

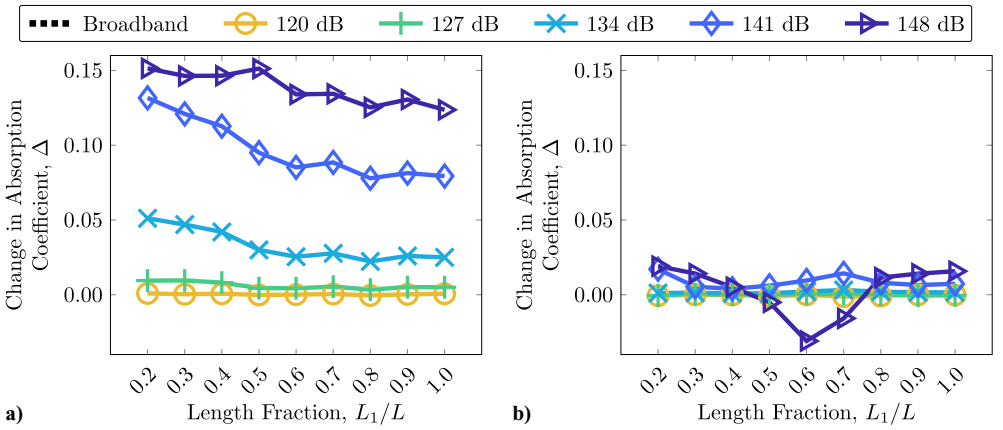

Fig. 12 Change in QWR peak absorption coefficients with discrete tone ISPL at a) fundamental and b) first harmonic.

The absorption coefficient of a resonator will be maximized when its normalized impedance is unity [4,22]. Figure 13 shows the normalized acoustic resistance (the real part of the impedance) at the resonance frequencies of the QWR for all length fractions as a function of the ISPL. Given this quantity, the nonmonotonic trend in the absorption coefficient at the QWR first harmonic, shown in Fig. 11b, can be readily interpreted. The acoustic reactance (the imaginary part of the impedance) is zero, and so not shown, at the QWR's resonance frequencies. Figure 13a shows the normalized resistance for the fundamental resonance frequency, and the values at the first harmonic are shown in Fig. 13b.

In summary, the acoustic resistance increases with ISPL at both resonance frequencies, as expected. At the QWR's fundamental resonance frequency, these increases in ISPL brought the resistance from $\theta \approx 0.4$ for the 120 dB ISPL closer to the optimal value of $\theta = 1$, which would give an absorption coefficient of 1. For the first harmonic, the resistance for the low-amplitude, broadband noise began closer to 1. The resistance of the QWR increases monotonically with ISPL and exceeds 1 as the ISPL is increased to 148 dB ISPL. This leads to the absorption peak at the first harmonic increasing and decreasing with increasing ISPL. The resistance is greatest when the bend is placed where relatively high acoustic velocities are expected (see Fig. 3).

C. Direct Numerical Simulation

The simulation results presented here confirm the interpretations of the experimental results via a two-dimensional model solution. This comparison establishes a link between the placement of a bend along a QWR and the acoustically induced vortex formation near the bend.

Figure 14 shows the absorption performance results at the QWR's fundamental resonance frequency (1 kHz) as a function of bend location for ISPLs of 120 and 148 dB. Figure 14a shows the absorption coefficient. The absorption is higher when the bend is closer to the resonator inlet. Figure 14b shows the change in absorption coefficient relative to the 90 dB OISPL case (broadband noise). This result is similar to the experimental results in Fig. 12a, showing that the degree of nonlinearity exhibited by the QWR (as indicated by Δ) for 148 dB depends on the bend location.

Figure 15 shows the time-averaged vorticity distributions over 50 acoustic cycles near the resonator inlet for $L_1/L = 1.0$. To the left of the resonator inlet, the vorticity inside the impedance tube is very chaotic, as expected. As such, the expected value of the vorticity contains faint traces of the many vortices produced during acoustic outflow from the resonator across the entire simulation. The vorticity generated inside the resonator near the inlet is comparable across all three length fractions simulated. However, differences between the QWRs of varying length fractions are evident when inspecting the vorticity near the internal bend.

Time-averaged vorticity fields over 50 cycles near the bend are shown for an ISPL of 120 dB in Fig. 16. A greater vorticity is observed for $L_1/L = 0.4$ than for $L_1/L = 0.8$. This result is expected because of the greater acoustic velocity fluctuations near the bend for lower L_1/L at the fundamental resonance frequency, as described in Sec. II. Although vortex formation occurs near the bend, it is localized, and the associated dissipation may scale linearly with the ISPL; the absorption coefficient at this ISPL was approximately equal to that at 90 dB OISPL (broadband noise). This result suggests that vortex formation can occur even for low amplitudes where the QWR behaves linearly. Figure 17 shows similar results for an ISPL of 148 dB. The vorticity near the bend is greater

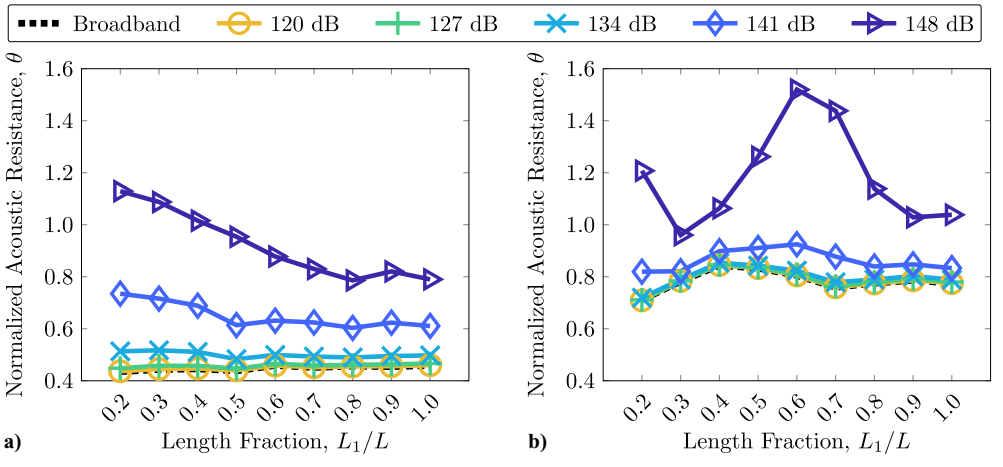

Fig. 13 Normalized acoustic resistance as a function of discrete tone ISPL for the a) fundamental resonance frequency and b) first harmonic.

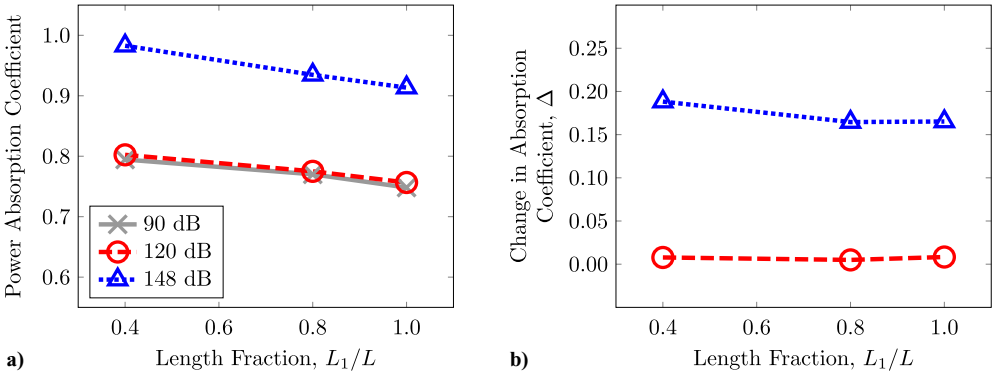

Fig. 14 Simulated 2D QWR performance along three different bend locations at the fundamental frequency for a) peak absorption coefficients and b) change in peak absorption coefficients relative to the 90 dB baseline.

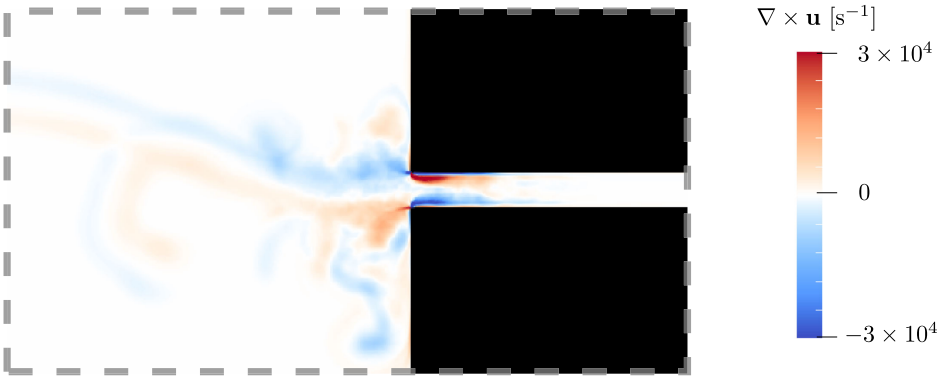

Fig. 15 Time-averaged vorticity distribution near the resonator inlet under a 1 kHz tone with incident SPL of 148 dB.

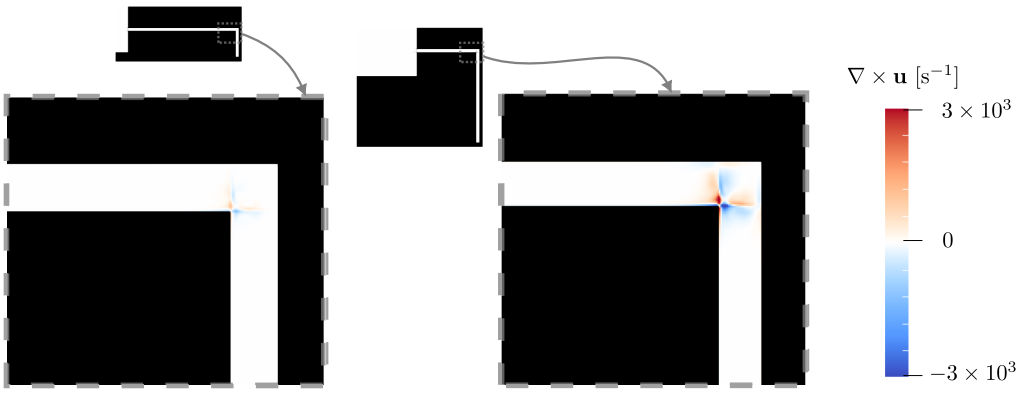

Fig. 16 Time-averaged vorticity distribution for a) $L_1/L = 0.8$ and b) $L_1/L = 0.4$ near the bend under a 1 kHz tone with incident SPL 120 dB.

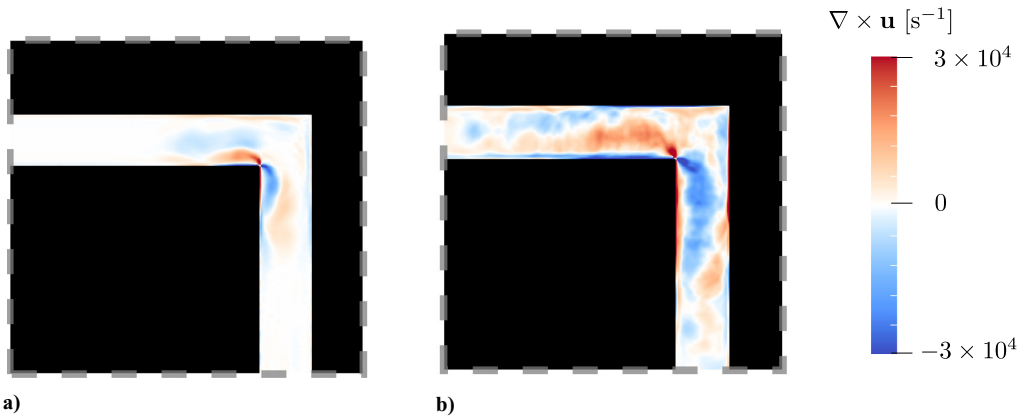

Fig. 17 Time-averaged vorticity distribution for a) $L_1/L = 0.8$ and b) $L_1/L = 0.4$ near the bend under a 1 kHz tone with incident SPL of 148 dB.

for this higher ISPL. (The color scale used for this figure spans an order of magnitude greater than Fig. 16.) Further, the vorticity is no longer localized near the bend. Along with this more vigorous vortex formation, the QWR power absorption coefficient increases by more than 0.15. Similarly as in the 120 dB case, the vorticity for the $L_1/L = 0.4$ QWR is greater than that for the $L_1/L = 0.8$ QWR.

V. Conclusions

This study examined the effects of the location of a sharp, 90 deg bend on the performance of QWRs. In the presence of low-amplitude, broadband noise (ISPL less than 100 dB re 20 μPa) the location of the 90 degree bend had little effect on the resonance frequencies and absorption coefficient, which did not change more than approximately 4 to 2%, respectively, relative to the lowest value. A dependence of the resonance frequency on bend location was nonetheless recognized, in which the resonance frequency increases with the magnitude of acoustic velocity fluctuations near the bend within the QWR. This result holds for at least the fundamental and first harmonic. Future research is required to observe QWR behavior at even higher harmonics.

In the presence of high-amplitude, discrete tones between 120 and 148 dB, the location of the bend impacted QWR performance. The QWRs exhibited varying degrees of nonlinearity depending on the bend location. The degree of nonlinearity was greatest when the bend was located where acoustic velocity fluctuations within the QWR are expected to be the highest. The acoustic velocities, the driving factor for vortex formation discussed in this paper, are largest near the QWR inlet at its fundamental resonance frequency. Therefore, at the fundamental level, the closer a 90 deg bend is placed to the inlet, the greater the nonlinearity is found to be. We observed a similar trend for the first harmonic.

The two-dimensional DNS results agree with the experiments that nonlinear effects are greater for bends placed where relatively high acoustic velocities are expected. For the model cases at the fundamental resonance frequency shown in this paper, bends placed closer to the resonator inlet are paired with greater nonlinearities, as demonstrated by increased vorticity generation around these bends at high ISPL conditions. Nonlocal vortex formation under high ISPL indicates that vorticity does not dissipate immediately at the bend.

Though some trends in the measured absorption coefficients were difficult to interpret, a simple statement can be made regarding the impedance of the QWRs. In all cases, the QWR acoustic resistance θ at a given resonance frequency increases with ISPL. This increase was largest when a bend was located where acoustic velocities are expected to be highest along the QWR channel. For the QWR's fundamental resonance frequency, a larger absorption coefficient with ISPL was observed for all ISPL cases. For the first harmonic, the absorption coefficient increased to 1 (normalized resistance approached 1) and subsequently decreased to lower values with increasing ISPL (normalized resistance increased beyond 1). These results imply that a bent QWR can perform better (greater absorption) or worse (less absorption) than an equivalent, straight QWR, depending on whether its acoustic resistance is greater than or less than 1. These effects should be considered when designing variable-depth liners with bent channels to achieve maximum sound absorption.

It is recommended that similar future research be conducted where the presence of a realistic liner *face sheet* is included on the incident face of the QWR. For a series of resonator/face sheet combinations that are well designed (i.e., providing a high absorption coefficient at the QWR's fundamental resonance frequency), the relative importance of dissipation of sound along the QWR's interior walls and in/around face sheet is expected to change. For example, a well-designed QWR with a face sheet installed could possess lower velocities inside the QWR channel than without the face sheet, and thus the nonlinearities discovered in this paper may only be evident at even higher ISPLs. Future work on the role that the QWR's bend angle and cross-sectional dimensions have on the issues studied in this paper would also be of interest.

Acknowledgments

The second author, D.N.R., was partially supported by the National Science Foundation Graduate Research Fellowship under grant number DGE-2039655. For the computational effort, this work used NCSA Delta through allocation TG-PHY210084 (PI Bryngelson) from the Advanced Cyberinfrastructure Coordination Ecosystem: Services & Support (ACCESS) program, which is supported by National Science Foundation grant numbers 2138259, 2138286, 2138307, 2137603, and 2138296. H.Y. acknowledges the use of computational resources at Georgia Institute of Technology, including PACE Phoenix. The authors are grateful to the Georgia Tech Research Institute for providing access to its facilities, which enabled the completion of this work. They are particularly grateful to Principal Research Engineer Robert Funk (Georgia Tech Research Institute) for valuable support with the experimental facilities. We thank graduate student Michael Milone for his helpful review and thoughtful suggestions, which improved the quality of this paper. Any opinion, findings, and conclusions or recommendations expressed in this material are those of the authors and do not necessarily reflect the views of the National Science Foundation.

References

[1] Oberg, C. L., "Combustion Stabilization with Acoustic Cavities," *Journal of Spacecraft and Rockets*, Vol. 8, No. 12, 1971, pp. 1220–1225. https://doi.org/10.2514/3.30366

[2] Zhao, D., and Li, X., "A Review of Acoustic Dampers Applied to Combustion Chambers in Aerospace Industry," *Progress in Aerospace Sciences*, Vol. 74, April 2015, pp. 114–130. https://doi.org/10.1016/j.paerosci.2014.12.003

[3] Förner, K., Cárdenas Miranda, A., and Polifke, W., "Mapping the Influence of Acoustic Resonators on Rocket Engine Combustion Stability," *Journal of Propulsion and Power*, Vol. 31, No. 4, 2015, pp. 1159–1166. https://doi.org/10.2514/1.B35660

[4] Lympany, S., "Acoustic Damping Mechanisms of Half-Wave Resonators in a Rocket Engine Environment," Ph.D. Dissertation, School of Aerospace Engineering, Georgia Inst. of Technology, Atlanta, GA, 2018. ProQuest Dissertations & Theses.

[5] Yu, J., and Chien, E., "Folding Cavity Acoustic Liner for Combustion Noise Reduction," *12th AIAA/CEAS Aeroacoustics Conference (27th AIAA Aeroacoustics Conference)*, AIAA Paper 2006-2681, 2006. https://doi.org/10.2514/6.2006-2681

[6] Sutliff, D. L., and Jones, M. G., "Low-Speed Fan Noise Attenuation from a Foam-Metal Liner," *Journal of Aircraft*, Vol. 46, No. 4, 2009, pp. 1381–1394. https://doi.org/10.2514/1.41369

[7] Jones, M. G., Simon, F., and Roncen, R., "Broadband and Low-Frequency Acoustic Liner Investigations at NASA and ONERA," *AIAA Journal*, Vol. 60, No. 4, 2022, pp. 2481–2500. https://doi.org/10.2514/1.J060862

[8] Galles, M. B., Nark, D. M., Jones, M. G., and Greenwood, E., "Optimization of Variable Depth Acoustic Liners with Grazing Flow," *AIAA SCITECH 2024 Forum*, AIAA Paper 2024-2803, 2024. https://doi.org/10.2514/6.2024-2803

[9] Wirt, L. S., "Sound Absorptive Materials to Meet Special Requirements," *Journal of the Acoustical Society of America*, Vol. 57, No. 1, 1975, pp. 126–143. https://doi.org/10.1121/1.380423

[10] Kreitzman, J., and Jones, M. G., "An Experimental and Predictive Study of Bent-Chamber Acoustic Liners," NASA TM 20240001001, 2024.

[11] Jones, M. G., and Howerton, B. M., "Evaluation of Novel Liner Concepts for Fan and Airframe Noise Reduction," *22nd AIAA/CEAS Aeroacoustics Conference*, AIAA Paper 2016-2787, 2016. https://doi.org/10.2514/6.2016-2787

[12] Chambers, A. T., Manimala, J. M., and Jones, M. G., "Design and Optimization of 3D Folded-Core Acoustic Liners for Enhanced Low-Frequency Performance," *AIAA Journal*, Vol. 58, No. 1, 2020, pp. 206–218. https://doi.org/10.2514/1.J058017

[13] Kumar, S., and Lee, H. P., "Labyrinthine Acoustic Metastructures Enabling Broadband Sound Absorption and Ventilation," *Applied Physics Letters*, Vol. 116, No. 13, 2020, Paper 134103. https://doi.org/10.1063/5.0004520

[14] Catapane, G., Magliacano, D., Petrone, G., Casaburo, A., Franco, F., and De Rosa, S., "Labyrinth Resonator Design for Low-Frequency Acoustic Meta-Structures," *International Conference on Wave Mechanics and Vibrations*, Vol. 125, Springer, Berlin, 2022, pp. 681–694. https://doi.org/10.1007/978-3-031-15758-5_70

[15] Ramsey, D. N., Filoon, J., and Ahuja, K. K., "Broadening the Bandwidth of Resonant Sound Absorbers Using Space-Coiling Acoustic Metamaterials," *AIAA SCITECH 2022 Forum*, AIAA Paper 2022-2558, 2022. https://doi.org/10.2514/6.2022-2558

[16] Li, Y., Yu, G., Liang, B., Zou, X., Li, G., Cheng, S., and Cheng, J., "Three-Dimensional Ultrathin Planar Lenses by Acoustic Metamaterials," *Scientific Reports*, Vol. 4, No. 1, 2014, p. 6830. https://doi.org/10.1038/srep06830

[17] Liang, Z., and Li, J., "Extreme Acoustic Metamaterial by Coiling Up Space," *Physical Review Letters*, Vol. 108, No. 11, 2012, Paper 114301. https://doi.org/10.1103/PhysRevLett.108.114301

[18] Li, Y., Liang, B., Gu, Z.-M., Zou, X.-Y., and Cheng, J.-C., "Reflected Wavefront Manipulation Based on Ultrathin Planar Acoustic Metasurfaces," *Scientific Reports*, Vol. 3, No. 1, 2013, p. 2546. https://doi.org/10.1038/srep02546

[19] Xie, Y., Popa, B.-I., Zigoneanu, L., and Cummer, S. A., "Measurement of a Broadband Negative Index with Space-Coiling Acoustic Metamaterials," *Physical Review Letters*, Vol. 110, No. 17, 2013, Paper 175501. https://doi.org/10.1103/PhysRevLett.110.175501

[20] Cummer, S. A., Christensen, J., and Alù, A., "Controlling Sound with Acoustic Metamaterials," *Nature Reviews Materials*, Vol. 1, No. 3, 2016, pp. 1–13. https://doi.org/10.1038/natrevmats.2016.1

[21] Cummings, A., "Sound Transmission in Curved Duct Bends," *Journal of Sounds and Vibration*, Vol. 35, Jan. 1974, pp. 451–477.

[22] Tang, Y., He, W., Xin, F., and Lu, T. J., "Nonlinear Sound Absorption of Ultralight Hybrid-Cored Sandwich Panels," *Mechanical Systems and Signal Processing*, Vol. 135, 2020, Paper 106428. https://doi.org/10.1016/j.ymssp.2019.106428

[23] Zhu, J., Qu, Y., Gao, H., and Meng, G., "Nonlinear Sound Absorption of Helmholtz Resonators with Serrated Necks Under High-Amplitude Sound Wave Excitation," *Journal of Sound and Vibration*, Vol. 537, July 2022, Paper 117197. https://doi.org/10.1016/j.jsv.2022.117197

[24] Sun, W., Chu, Z., and Lang, Y., "Nonlinear Sound Absorption of Coiling-up Space Under High Amplitude Acoustic Excitation," *Applied Acoustics*, Vol. 220, March 2024, Paper 109956. https://doi.org/10.1016/j.apacoust.2024.109956

[25] Blackstock, D. T., *Fundamentals of Physical Acoustics*, Wiley, Hoboken, NJ, 2000, pp. 322–327, 519–524.

[26] Bechert, D. W., "Sound Absorption Caused by Vorticity Shedding Demonstrated with a Jet Flow," *Journal of Sound and Vibration*, Vol. 70, No. 3, 1980, pp. 389–405. https://doi.org/10.1016/0022-460X(80)90307-7

[27] Cummings, A., and Eversman, W., "High Amplitude Acoustic Transmission Through Duct Terminations: Theory," *Journal of Sound and Vibration*, Vol. 91, No. 4, 1983, pp. 503–518. https://doi.org/10.1016/0022-460X(83)90829-5

[28] Salikuddin, M., and Ahuja, K. K., "Acoustic Power Dissipation on Radiation Through Duct Terminations: Experiments," *Journal of Sound and Vibration*, Vol. 91, No. 4, 1983, pp. 479–502. https://doi.org/10.1016/0022-460X(83)90828-3

[29] Disselhorst, J. H. M., and van Wijngaarden, L., "Flow in the Exit of Open Pipes During Acoustic Resonance," *Journal of Fluid Mechanics*, Vol. 99, No. 2, 1980, pp. 293–319. https://doi.org/10.1017/S0022112080000626

[30] Zhang, Q., and Bodony, D. J., "Numerical Investigation and Modelling of Acoustically Excited Flow Through a Circular Orifice Backed by a Hexagonal Cavity," *Journal of Fluid Mechanics*, Vol. 693, Jan. 2012, pp. 367–401. https://doi.org/10.1017/jfm.2011.537

[31] Martínez del Río, L., Málaga, C., Zenit, R., and Rendón, P. L., "Generation of Vorticity at the Open End of Acoustic Waveguides," *Physical Review Fluids*, Vol. 8, No. 5, 2023, Paper 053402. https://doi.org/10.1103/PhysRevFluids.8.053402

[32] Ingard, U., and Ising, H., "Acoustic Nonlinearity of an Orifice," *Journal of the Acoustical Society of America*, Vol. 42, No. 1, 1967, pp. 6–17. https://doi.org/10.1121/1.1910576

[33] Ingård, U., and Labate, S., "Acoustic Circulation Effects and the Nonlinear Impedance of Orifices," *Journal of the Acoustical Society of America*, Vol. 22, No. 2, 1950, pp. 211–218. https://doi.org/10.1121/1.1906591

[34] Tam, C. K. W., Kurbatskii, K. A., Ahuja, K. K., and Gaeta, R. J., Jr., "A Numerical and Experimental Investigation of the Dissipation Mechanisms of Resonant Acoustic Liners," *Journal of Sound and Vibration*, Vol. 245, No. 3, 2001, pp. 545–557. https://doi.org/10.1006/jsvi.2001.3571

[35] Förner, K., Temiz, M. A., Polifke, W., Arteaga, I. L., and Hirschberg, A., "On the Non-Linear Influence of the Edge Geometry on Vortex Shedding in Helmholtz Resonators," *Proceedings of the 22nd International Conference on Sound and Vibration (ICSV. 22)*, International Inst. of Acoustics and Vibration, July 2015, pp. 1–8.

[36] Welch, P., "The Use of Fast Fourier Transform for the Estimation of Power Spectra: A Method Based on Time Averaging over Short, Modified Periodograms," *IEEE Transactions on Audio and Electroacoustics*, Vol. 15, No. 2, 1967, pp. 70–73. https://doi.org/10.1109/TAU.1967.1161901

[37] ASTM, A., *E1050-12, Standard Test Method for Impedance and Absorption of Acoustical Materials Using a Tube, Two Microphones and a Digital Frequency Analysis System*, ASTM International, West Conshohocken, PA, 2012. https://doi.org/10.1520/E1050-12

[38] Bryngelson, S. H., Schmidmayer, K., Coralic, V., Meng, J. C., Maeda, K., and Colonius, T., "MFC: An Open-Source High-Order Multi-Component, Multi-Phase, and Multi-Scale Compressible Flow Solver," *Computer Physics Communications*, Vol. 266, Sept. 2021, Paper 107396. https://doi.org/10.1016/j.cpc.2020.107396

[39] Radhakrishnan, A., Le, Berre, Spratt, J.-S., Rodriguez, M., Jr., and Bryngelson, S. H., "Method for Scalable and Performant GPU-Accelerated Simulation of Multiphase Compressible Flow," *Computer Physics Communications*, Vol. 302, Sept. 2024, Paper 109238. https://doi.org/10.1016/j.cpc.2024.109238

[40] Wilfong, B., Le Berre, H. A., Radhakrishnan, A., Gupta, A., Vaca-Revelo, D., Adam, D., Yu, H., Lee, H., Chreim, J. R., Barbosa, M. C., et al., "MFC. 5.0: An Exascale Many-Physics Flow Solver," arXiv preprint arXiv: 2503.07953, 2025, Paper 110055. https://doi.org/10.1016/j.cpc.2026.110055

[41] Maeda, K., and Colonius, T., "A Source Term Approach for Generation of One-Way Acoustic Waves in the Euler and Navier–Stokes Equations," *Wave Motion*, Vol. 75, Dec. 2017, pp. 36–49. https://doi.org/10.1016/j.wavemoti.2017.08.004

[42] Tseng, Y.-H., and Ferziger, J. H., "A Ghost-Cell Immersed Boundary Method for Flow in Complex Geometry," *Journal of Computational Physics*, Vol. 192, No. 2, 2003, pp. 593–623. https://doi.org/10.1016/j.jcp.2003.07.024

[43] Bryngelson, S. H., Fox, R. O., and Colonius, T., "Conditional Moment Methods for Polydisperse Cavitating Flows," *Journal of Computational Physics*, Vol. 477, March 2023, Paper 111917. https://doi.org/10.1016/j.jcp.2023.111917

[44] Charalampopoulos, A., Bryngelson, S. H., Colonius, T., and Sapsis, T. P., "Hybrid Quadrature Moment Method for Accurate and Stable Representation of Non-Gaussian Processes and Their Dynamics," *Philosophical Transactions of the Royal Society A*, Vol. 380, No. 2229, 2022. https://doi.org/10.1098/rsta.2021.0209

[45] Yu, H., Ahuja, K. K., Sankar, L. N., and Bryngelson, S. H., "Numerical Investigation of Leakage of High-Amplitude Sound in Ill-Fitting Earplugs," *AIAA AVIATION FORUM AND ASCEND 2024*, AIAA Paper 2024-4391, 2024. https://doi.org/10.2514/6.2024-4391

[46] Yu, H., Ahuja, K. K., Sankar, L. N., and Bryngelson, S. H., "Transmission of High-Amplitude Sound Through Leakages of Ill-Fitting Earplugs," arXiv preprint arXiv: 2510.16355, 2025.

[47] Tam, C. K. W., Ju, H., Jones, M. G., Watson, W. R., and Parrott, T. L., "A Computational and Experimental Study of Slit Resonators," *Journal of Sound and Vibration*, Vol. 284, Nos. 3–5, 2005, pp. 947–984. https://doi.org/10.1016/j.jsv.2004.07.013

[48] Tam, C. K. W., Ju, H., Jones, M. G., Watson, W. R., and Parrott, T. L., "A Computational and Experimental Study of Resonators in Three Dimensions," *Journal of Sound and Vibration*, Vol. 329, No. 24, 2010, pp. 5164–5193. https://doi.org/10.1016/j.jsv.2010.06.005

[49] Cambonie, T., Gourdon, E., Redon, E., and Leclere, Q., "Influence of Right-Angled Elbows on the Modal Response of Labyrinthine Meta-Materials," *Wave Motion*, Vol. 123, Dec. 2023, Paper 103228. https://doi.org/10.1016/j.wavemoti.2023.103228

[50] Cambonie, T., Mbailassem, F., and Gourdon, E., "Bending a Quarter Wavelength Resonator: Curvature Effects on Sound Absorption Properties," *Applied Acoustics*, Vol. 131, Feb. 2018, pp. 87–102. https://doi.org/10.1016/j.apacoust.2017.10.004

C. Bailly
Associate Editor